Supporting Information

Engineering Magnetosome for High-Performance Cancer Vaccination

Feng Li[†], *Weidong Nie*[†], *Fan Zhang*[†], *Guihong Lu*[†], *Chengliang Lv*[†], *Yanlin Lv*[‡], *Weier Bao*[‡,§], *Lijun Zhang*[‡,§], *Shuang Wang*[‡], *Xiaoyong Gao*[‡], *Wei Wei**[,‡,§] and *Hai-Yan Xie**[,†]

[†]School of Life Science, Beijing Institute of Technology, Beijing, 100081, P.R.China

[‡]State Key Laboratory of Biochemical Engineering, Institute of Process Engineering, Chinese Academy of Sciences, Beijing, 100190, P.R.China

[§] University of Chinese Academy of Sciences, Beijing, 100049, P.R.China

Part I: Experimental Section

Cell lines: 4T1 murine breast tumor cells and Luc-4T1 murine breast tumor cells were purchased from Peking Union Medical College Hospital (Beijing, China). These cells were cultured in media supplemented with 10% FBS and 1% penicillin-streptomycin at 37 °C with 5% CO_2, and were passaged at approximately 80% confluency.

Animals: Four-week-old BALB/c mice (14-18 g, female) were obtained from Vital River laboratories (Beijing, China). All animal experiments were performed in accordance with the guide for the Care and Use of Laboratory Animals and were approved by the Experimental Animal Ethics Committee in Beijing.

Antibody modification: Anti-mouse CD205 antibody (Ab) was incubated with a 50-fold molar excess of NHS-PEG_5-DBCO (A134-10, ClickChemistryTools, USA) at 4 °C overnight. The prepared DBCO-Anti-CD205 (DBCO-Ab) was purified through filtering at 7000 g for 50 min at 4 °C (Amicon® Ultra-0.5, Millipore Co, German) and then resuspended in PBS and analyzed by matrix-assisted laser desorption ionization time of flight mass spectrometry (MALDI-TOF MS, AXIMA-Pertormance MA, SHIMADZU, Japan). The activity of DBCO-Ab was investigated through fluorescence microscopy imaging and flow cytometry analysis. For fluorescence microscopy imaging, bone marrow-derived dendritic cells (BMDCs) were prepared as described previously. Then BMDCs were plated on 35 mm glass-bottom dishes at a density of 3×10^5 cells. After incubation for 24 h, the cells were fixed with 4% paraformaldehyde and then blocked with 5% BSA solution. The resulting cells were incubated with anti-mouse CD205 or DBCO decorated anti-mouse CD205 at 37 °C for 1 h. After having been washed with PBS, they were incubated with DyLight 488-conjugated anti-rat secondary antibody, followed with fluorescence microscopy imaging. The fluorescence of DyLight 488-labeled cells was excited with an argon laser at 488

nm, and the emission was detected at 510-550 nm. For flow cytometry analysis, approximately 1 × 10^6 BMDCs were resuspended in cold PBS and incubated with anti-mouse CD205 or DBCO-Ab for 45 min at 4 °C. Then, the cells were incubated with DyLight 488-conjugated secondary antibody and analyzed with a flow cytometer (CyAn ADP, Beckman Coulter, USA).

Characterization of A/M/C-MNC: Dynamic light scattering (Malvern ZEN 3600 Zetasizer, UK) was used to measure the size and surface zeta potential of the formulations. DBCO-Ab decorated M/C-MNC (A/M/C-MNC) was suspended in PBS (pH 7.4) at a final concentration of 100 μg/mL, and then the size and zeta potential were measured every day for two weeks. The relaxivities and R_2 (spin-spin relaxation rate, $1/T_2$) were measured at 7 T using a 7 T Bruker pharmascan animal instrument (Bruker Optics, Tsukuba, Japan). MR images of each phantom were obtained on a 7 T superconducting magnet with T_2-weighted (3000/13.2) spin-echo sequences. The spacial resolution of the magnetic field we used was 136.72 μm, which wasmall enough for lymph nodes (~2 mm) observation. For fluorescence microscopy imaging, CpG-ODN, membrane and DBCO-anti-CD205 were individually labeled with FAM, 1,1'-Dioctadecyl-3,3,3',3'-tetramethylindodicarbocyanine (DiD) and a fluorescence secondary antibody, respectively. Then, the final A/M/C-MNC was imaged using a laser scanning confocal imaging system (Leica, USA). For SDS-polyacrylamide gel assays, whole 4T1 cells, membrane fragments, and M/C-MNC were prepared in an equal protein dose as measured by a BCA kit. Then, the samples were individually loaded in the wells of a 10% SDS-polyacrylamide gel and run at 120 V for 2 h.

Optimization of magnetic field administration: For magnetic field applied at different lymph nodes, BALB/c mice were individually injected subcutaneously at the tailbase with 100 μg DiD-labeled A/M/C-MNC then divided into three groups and the three groups were administrated magnetic field at inguinal lymph nodes, submaxillary lymph nodes and without magnetic field

application, respectively. All the lymph nodes were collected and analyzed by the *ex*/*in vivo* imaging system (FX Pro, Kodak, Japan). Then these lymph nodes were triturated into single cell suspensions and stained with FITC-conjugated anti-mouse CD11c, eFlour 450-conjugated anti-mouse CD8a, PE-conjugated anti-mouse CD40, APC/Cy7-conjugated anti-mouse CD86, PerCP/eFlour 710-conjugated anti-mouse MHC I and BV605-conjugated anti-mouse MHC II at 4 °C for 30 min. Then, the cells were dispersed in 500 μL of PBS and analyzed by flow cytometry. For magnetic field application at different time point, BALB/c mice were individually injected subcutaneously at the tailbase with 100 μg DiD- labeled A/M/C-MNC then divided into 8 groups. These groups were administrated with magnetic field at inguinal lymph nodes at 0 h, 0.5 h, 1 h, 2 h, 6 h, 12 h, 24 h and 48 h after vaccination, respectively. Then at 48 h after injection, they were treated follow the same methods as above. For magnetic field application lasting for different periods, BALB/c mice were individually injected subcutaneously at the tailbase with 100 μg DiD-labeled A/M/C-MNC and administrated magnetic field at inguinal lymph nodes. Then they were divided into 4 groups. The magnetic field application lasted for 0 d, 3 d, 7 d and 10 d, respectively. Then at 10 d after injection, they were treated follow the same methods as above.

Tumor prevention study in the 4T1 tumor model: BALB/c mice were vaccinated with PBS, MF, M/MNC, M/C-MNC, A/M/C-MNC or A/M/C-MNC(m) (100 μg MNC/mouse or equivalent) at tail base on day 10 and day 3. Then on day 0, they were inoculated with 5×10^5 4T1 cells at the ventral mammary fat pad. The tumor size of the mice was observed every two days. The experimental endpoint was defined as either death or a tumor size greater than 1000 mm^3. To analyze the survival, the same treatments of mice were administrated as above and the survival was observed every two days.

Anti-tumor study in 4T1 tumor model: BALB/c mice were inoculated subcutaneously with 5×10^5 4T1 cells at the ventral mammary fat pad on day 0. Then they were randomly divided into 7 groups: PBS, MF, M/MNC, M/C-MNC, A/M/C-MNC, A/M/C-MNC(m) and A/M/C-MNC(m)+aP. Each group was treated with the corresponding formulations at tail base on days 3 and 10. The aP was administered intraperitoneally on the same days at a dose of 200 μg/mouse. Tumor size, body weight and temperature were measured every two days and the experimental endpoint was defined as either death or tumor size greater than 1000 mm^3. Then, the lungs and hind legs of each mouse were collected to study the metastasis originated from the primary tumor. The tibia metastasis were imaged by computed tomography (CT). To analyze the survival, the same treatments of mice were administrated as above and the survival was observed every two days.

Anti-metastasis study in Luc-4T1 tumor model: BALB/c mice were divided into 7 groups: PBS, MF, M/MNC, M/C-MNC, A/M/C-MNC, A/M/C-MNC(m) and A/M/C-MNC(m)+aP, and then individually vaccinated with the corresponding formulation (100 μg MNC/mouse or equivalent) at tail base on day -10 and day -3. Then, on day 0, they were intravenously injected with Luc-4T1 cells (3×10^5 cells/mouse), and lung metastasis was imaged by IVIS Spectrum (PerkinElmer, USA) after an intraperitoneal injection with D-Luciferin sodium salt at a dose of 3 mg/mouse. The lungs of mice were collected at day 10. To analyze the survival, the same treatments of mice were administrated as above and the survival was observed every two days.

Postoperation recurrence inhibition effect: BALB/c mice were subcutaneously inoculated with 5×10^5 Luc-4T1 cells at the ventral mammary fat pad. Then on day 3, the tumors were surgically resected when the tumor volume reached 500 mm^3. On day 0 and 7, the mice were treated with PBS, MF, M/MNC, M/C-MNC, A/M/C-MNC, A/M/C-MNC(m) or A/M/C-MNC(m)+aP (100 μg

MNC/mouse or equivalent) at tail base. The primary tumors and the recurrent tumors were imaged by IVIS Spectrum (PerkinElmer, USA) after intraperitoneally injection with D-Luciferin sodium salt at a dose of 3 mg/mouse. The recurrent tumor sizes and survival were measured every two days and the experimental endpoint was defined as either death or tumor size greater than 1000 mm^3.

Long term immune memory effects of vaccine: BALB/c mice were inoculated subcutaneously with 5×10^5 Luc-4T1 cells at the ventral mammary fat pad on day 0. Then they were vaccinated subcutaneously at tail base with PBS, MF, M/MNC, M/C-MNC, A/M/C-MNC, A/M/C-MNC(m) or A/M/C-MNC(m)+aP (100 μg MNC/mouse or equivalent) on day 3 and 10. Then the primary tumors were surgically resected on day 14. Two weeks later, these mice were rechallenged with 1×10^5 Luc-4T1 cells into the right flank of each mouse. The primary tumors and the distant tumors were imaged by IVIS Spectrum (PerkinElmer, USA) after intraperitoneally injection with D-Luciferin sodium salt at a dose of 3 mg/mouse. The distant tumor sizes and survival were measured every two days and the experimental endpoint was defined as either death or tumor size greater than 1000 mm^3. To analyze the memory T cells, the same treatments of mice were administrated as above and the memory T cells were analyzed by flow cytometry on day 28.

Safety Estimation: For humane reasons, animals were sacrificed when the implanted tumor volume reached 1000 mm^3. The tissue sections of the hearts, livers, spleen, lung, and kidneys were stained with H&E (hematoxylin/eosin) and analyzed by light microscopy for post-mortem histopathology analysis. The serum levels of urea nitrogen (BUN), lactate dehydrogenase (LDH), alanine aminotransferase (ALT), aspartate transaminase (AST) and alkaline phosphatase (ALP) were analyzed spectrophotometrically using an automated analyzer (Hitachi-917, Hitachi Ltd.,

Tokyo, Japan). The serum cytokines were analyzed on day 18 using commercially available enzyme-linked immunosorbent assay kits.

Part II: Supplementary Text

We studied the *in vivo* prophylactic effects by immunizing mice with the different formulations before challenging them with 4T1 cells injected in the mammary fat pad (Figure S11A). Compared to the PBS group, vaccination with free MF or M/MNC failed to yield a noticeable reduction in tumor size (Figure S11B). This could be ameliorated when CpG-ODN was integrated in the magnetosome (M/C-MNC). Upon immunization with A/M/C-MNC, a significant delay in tumor growth was observed. Furthermore, with magnetic retention at the lymph nodes, tumor development could be almost completely suppressed in the A/M/C-MNC(m) group. Correspondingly, we observed very distinct tumor burdens 80 days posttreatment with the different prophylactic immunizations. As shown in the excised tumor images (Figure S11C), the tumor size gradually decreased in the order of PBS, MF, M/MNC, M/C-MNC, A/M/C-MNC, and A/M/C-MNC(m). Notably, in the A/M/C-MNC(m) group, only one mouse suffered from a very low tumor burden, while the other mice remained tumor free. The superior prophylactic performance of the A/M/C-MNC(m) group was also verified by survival time analysis, wherein no deaths occurred during the 80-day observation period (Figure S11D).

Part III: Figures

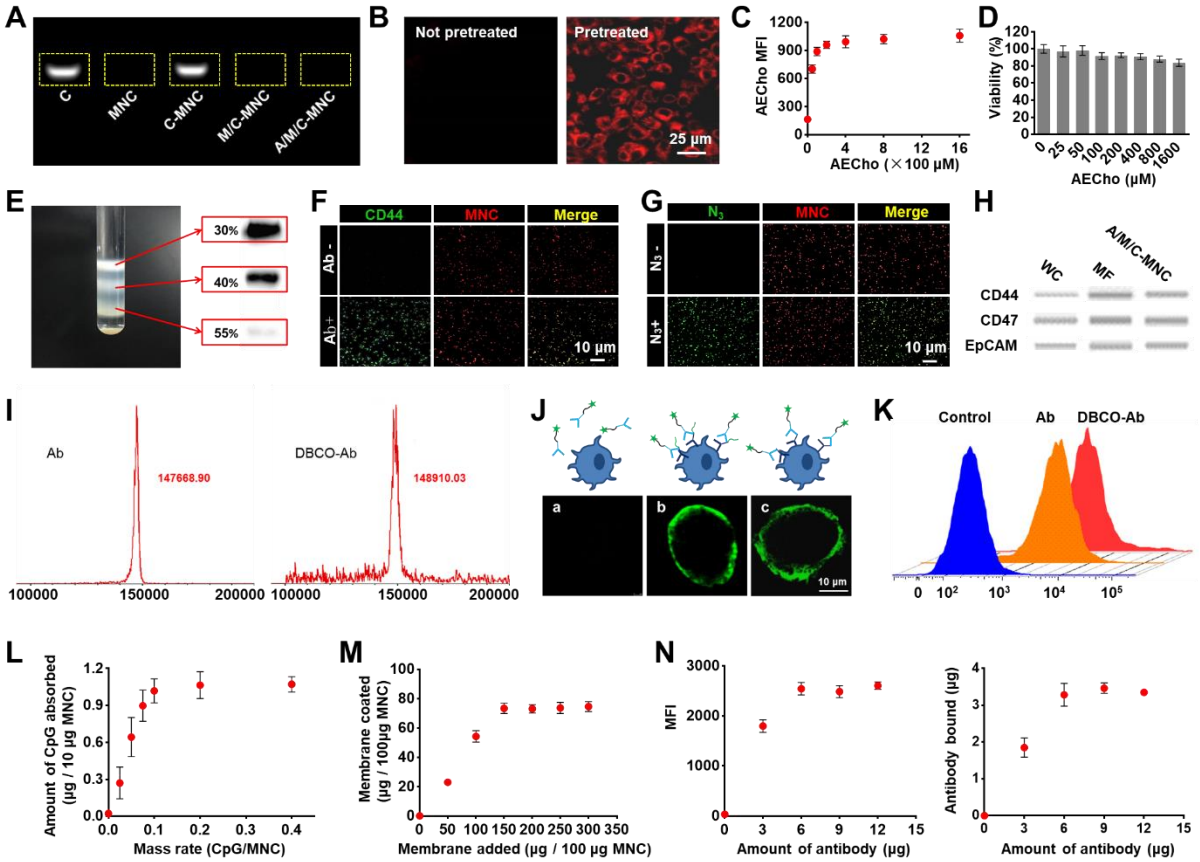

Figure S1. Construction and characterization of A/M/C-MNC. (A) Electrophoresis assay of free CpG-ODN (C), MNC, C-MNC, M/C-MNC and A/M/C-MNC. (B) Fluorescence images of AECho pretreated or not pretreated 4T1 cells after DBCO staining. (C) Fluorescence intensity of 4T1 cells pretreated with different concentrations of AECho. (D) Relative cell viability of 4T1 cells incubated with different concentrations of AECho. (E) Purification of 4T1 cell membranes. (F) Membrane coating confirmation by labeling the cytomembrane marker CD44. (G) Membrane coating confirmation by labeling azide groups on the membrane. (H) Membrane coating confirmation by western blotting of membrane marker, CD44, CD47 and EpCAM. (I) MALDI-TOF mass spectrometry of anti-CD205 antibody (Ab) before and after DBCO modification. The relative molecular weight increased by ~1241 Dalton, which corresponded to 1~2 DBCO. (J) DBCO-Ab activity confirmation by CLSM. A $CD8^+$ DCs incubated with the fluorescent secondary antibody only. B $CD8^+$ DCs sequentially incubated with DBCO-anti-CD205 and the fluorescent secondary antibody. C $CD8^+$ DCs sequentially incubated with anti-CD205 and the fluorescent secondary antibody. (K) DBCO-Ab activity confirmation by flow cytometry assays in (J). (L) Loading efficacy of CpG-ODN on MNC (10 μg). (M) Estimating the saturation coating of 4T1 cell membrane fragments on C-MNC (100 μg of MNC). (N) Estimating the saturation of DBCO-Ab on M/C-MNC (50 μg of MNC) through fluorescence spectral analysis (left) and protein quantification (right). When the amount of added DBCO-Ab became ~6 μg, the saturated decoration amount was ~3.4 μg. Bars represent the mean ± s.d. (n=3).

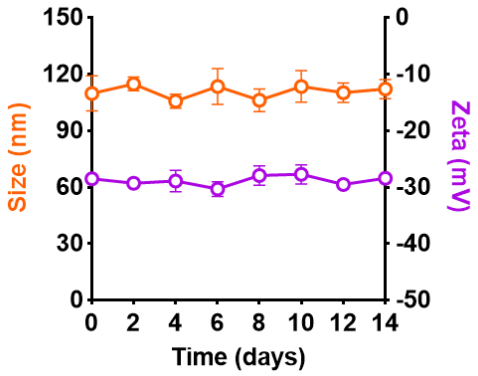

Figure S2. Stability of A/M/C-MNC over a 2-week period in culture medium. The result demonstrated the wonderful stability of A/M/C-MNC in the physiological environment.

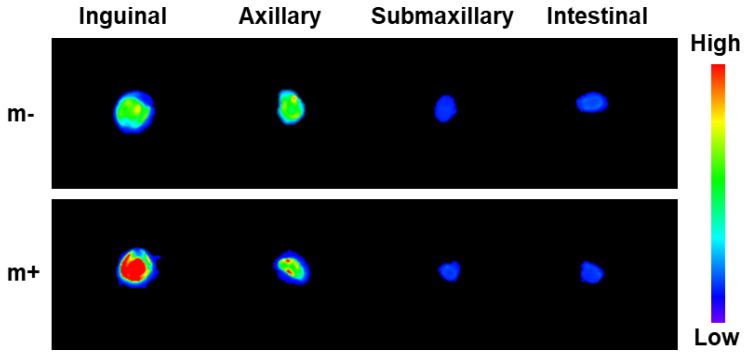

Figure S3. A/M/C-MNC distribution in different lymph nodes *in vivo*. The A/M/C-MNC was mainly drained to inguinal lymph nodes and axillary lymph nodes. Upon applying a magnetic field at the inguinal lymph node site, the accumulation of A/M/C-MNC in inguinal lymph node was increased while the other lymph nodes showed no changes.

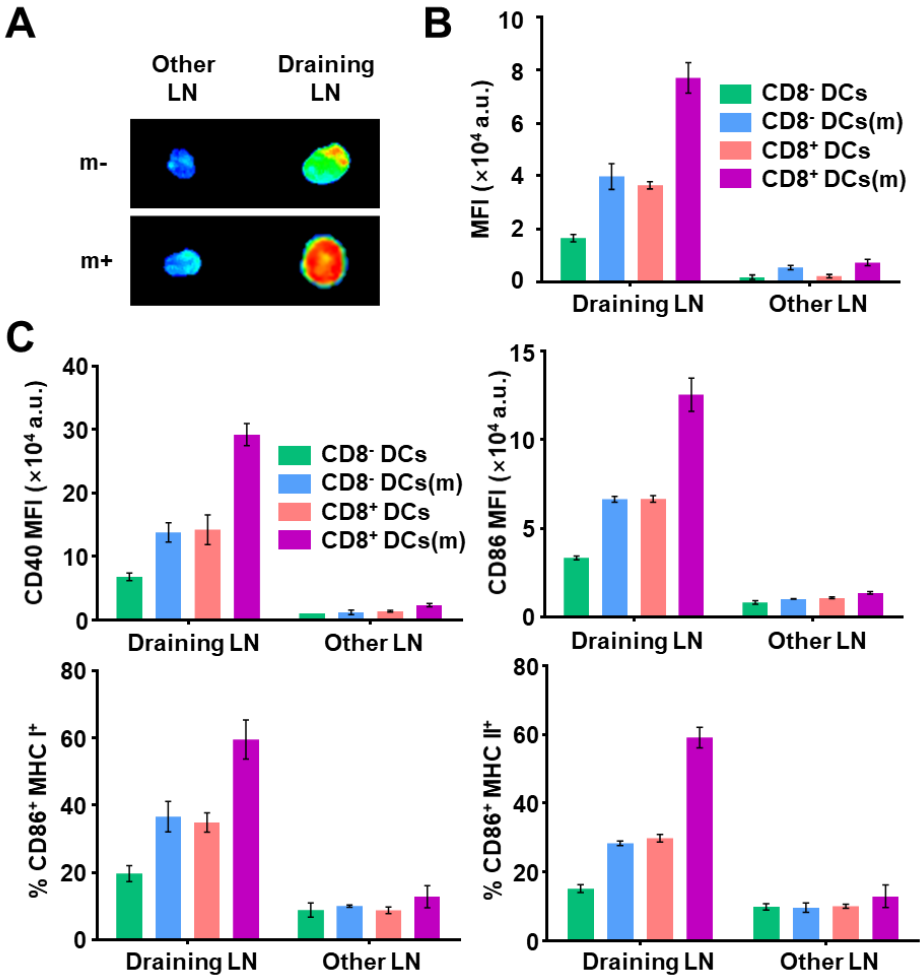

Figure S4. Retention of A/M/C-MNC and activation of DCs in different lymph nodes. (A) Fluorescence imaging of different lymph nodes after vaccination with DiD labeled A/M/C-MNC. The magnetic field was focused to the draining lymph node or the other lymph node. (B) MFI of DCs in the lymph nodes in (A). (C) Analysis of DC maturation markers CD40 and CD86, MHC-II and cross-presentation marker MHC-I in the lymph nodes in (A). All these results showed that the magnetic field had much nore effect in the draining lymph nodes than other lymph nodes, so the magnetic field should be focused to the draining lymph nodes. All data represent the mean ± s.d. (n = 3).

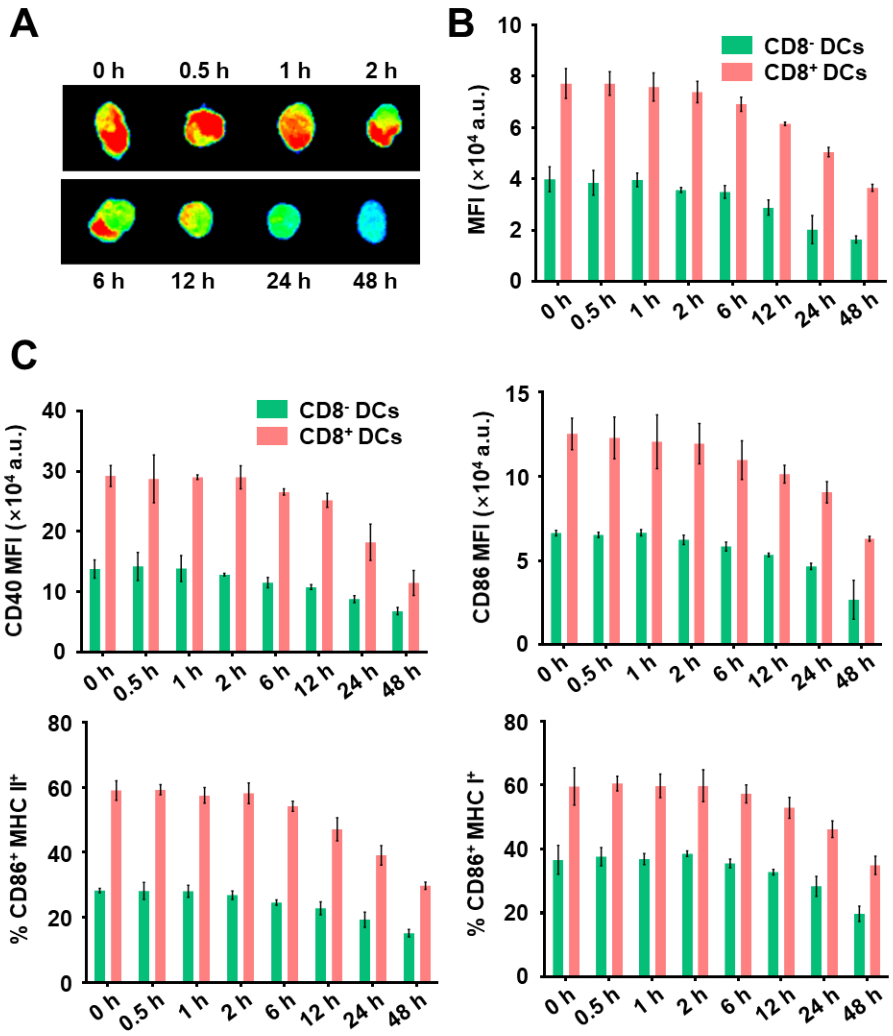

Figure S5. Retention of A/M/C-MNC and activation of DCs in the lymph nodes under magnetic field application began at different time. (A) Fluorescence imaging of the lymph nodes after vaccination with DiD labeled A/M/C-MNC. The magnetic field was applied at 0 h to 48 h after vaccination, respectively. (B) MFI of DCs in the lymph nodes in (A). (C) Analysis of DC maturation markers CD40 and CD86, MHC-II and cross-presentation marker MHC-I in the lymph nodes in (A). All these results presented that the retention effect reached the best when the magnetic field application began within 2 h after vaccination. All data represent the mean ± s.d. (n = 3).

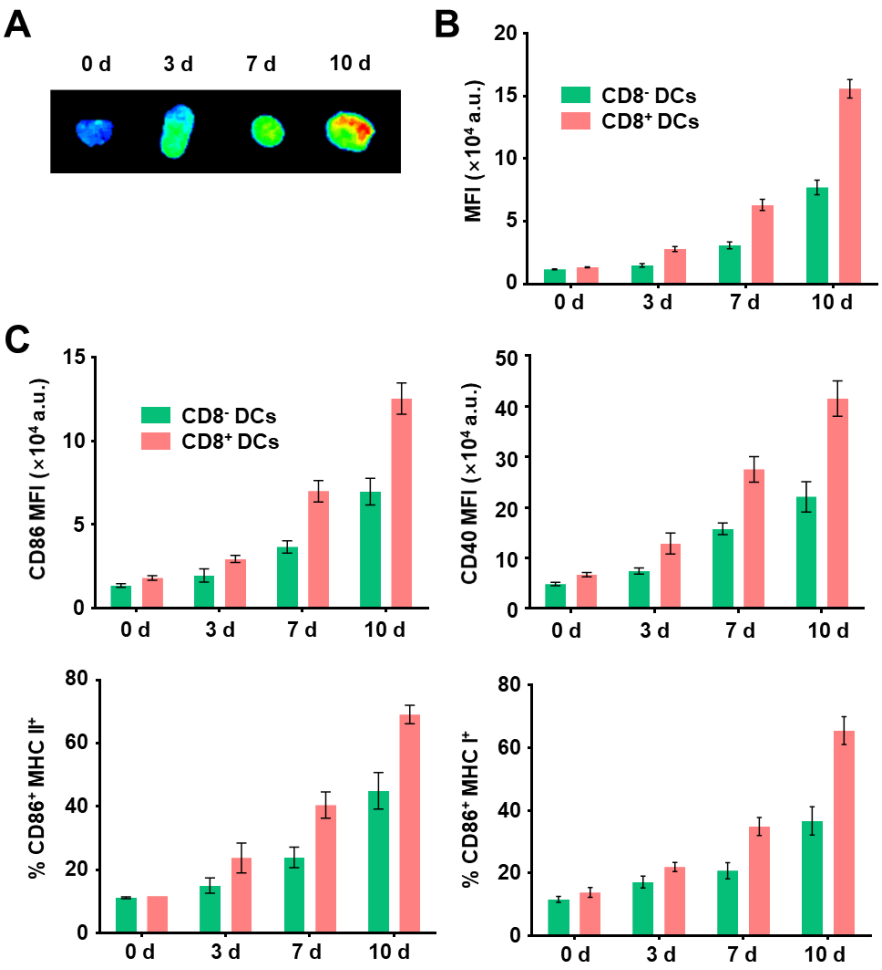

Figure S6. Retention of A/M/C-MNC and activation of DCs in the lymph nodes under magnetic field application lasted for different periods. (A) Fluorescence imaging of the lymph nodes after vaccination with DiD labeled A/M/C-MNC. The magnetic field application lasted for 0 d to 10 d, respectively. (B) MFI of DCs in the lymph nodes in (A). (C) Analysis of DC maturation markers CD40 and CD86, MHC-II and cross-presentation marker MHC-I in the lymph nodes in (A). All these results presented that the longer magnetic field lasted for, the better it worked. All data represent the mean ± s.d. (n = 3).

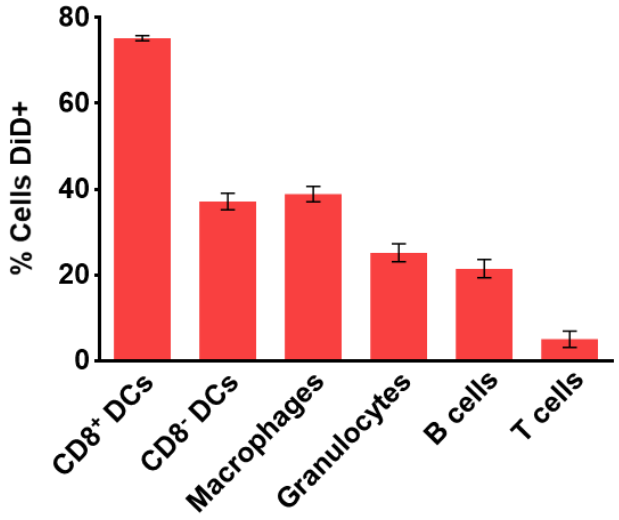

Figure S7. Uptake of A/M/C-MNC by different immune cells in the lymph nodes. A/M/C-MNC was preferably engulfed by $CD8^+$ DCs rather than other immune cells in the lymph node.

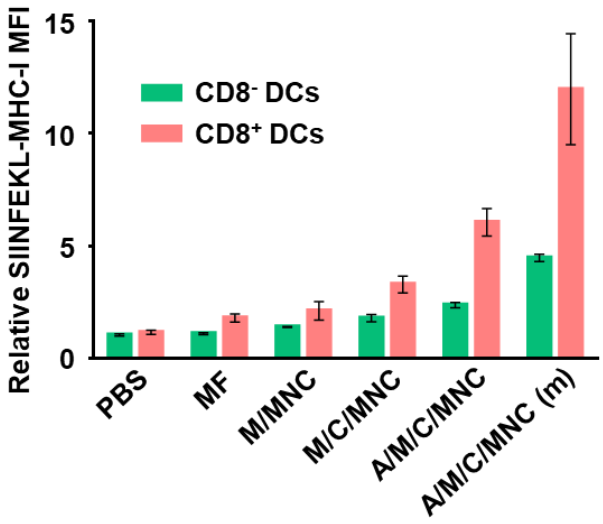

Figure S8. Anti-CD205-mediated cross-presentation of OVA by MHC I. Cross-presentation by MHC I in the lymph nodes was analyzed after vaccination with different EG7 membrane formulations. The epitope peptides (SIINFEKL, OVA257-264) were chosen as a representative antigen epitope. The SIINFEKL-MHC I expression in the lymph nodes gradually increased in the order of PBS, MF, M/MNC, M/C-MNC, A/M/C-MNC and A/M/C-MNC(m), which demonstrated the effective cross-presentation of cancer associated antigens by MHC I.

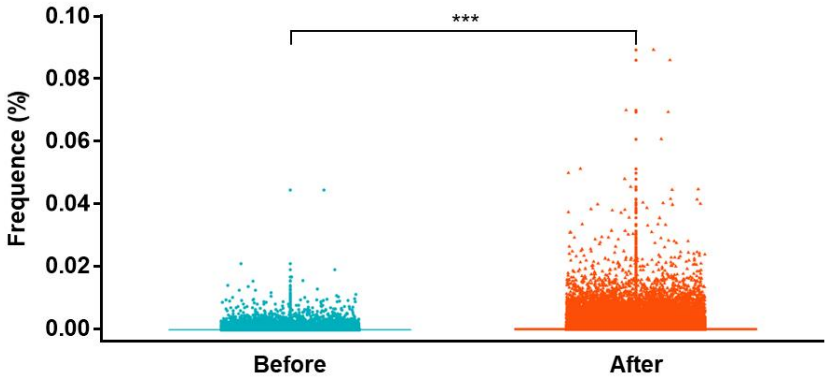

Figure S9. The frequencies of CDR3 sequence repertoire in the lymph nodes before and after vaccination. The statistics of CDR3 sequences indicated that the multi-antigenic cellular immune responses were aroused by our magnetosome vaccine.

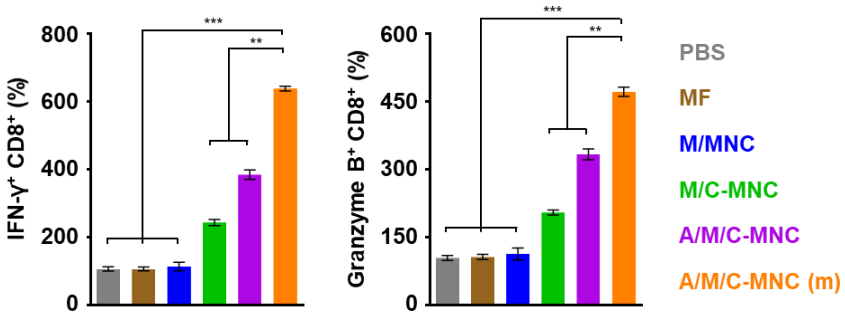

Figure S10. Relative percent of IFN-γ^+ $CD8^+$ T cells and Granzyme B^+ $CD8^+$ T cells in the lymph nodes after vaccination with different formulations.

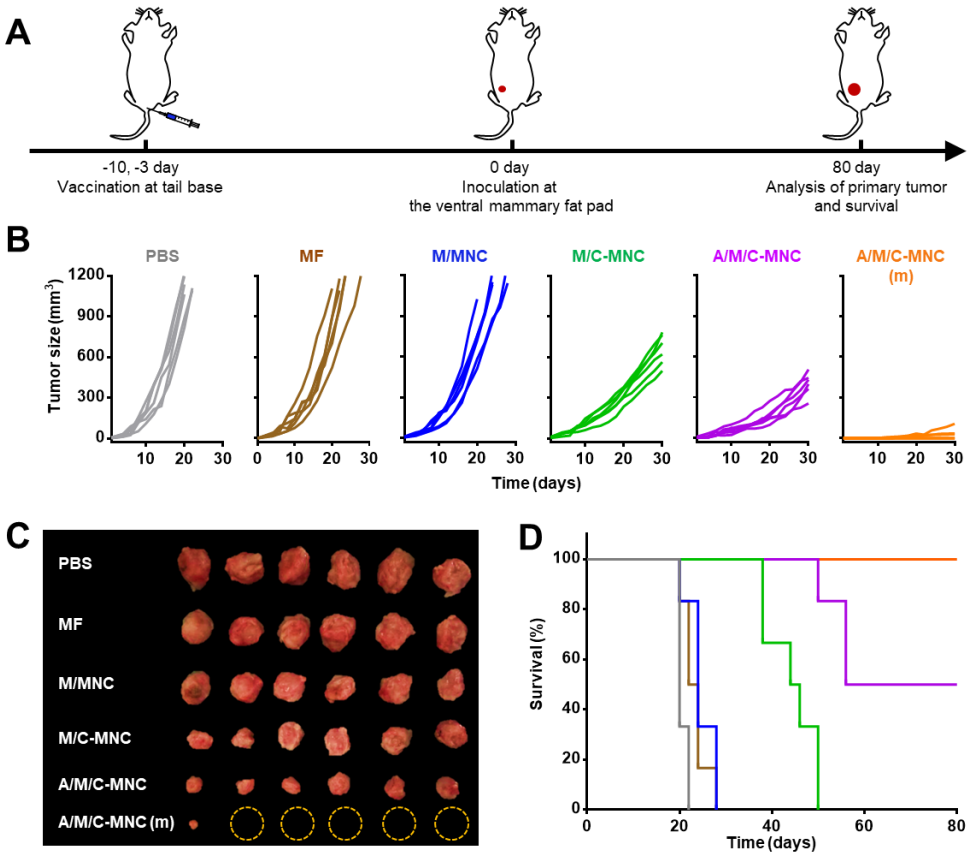

Figure S11. A/M/C-MNC-mediated prevention of tumorigenesis *in vivo*. (A) Treatment schedule for the prophylactic performance. (B) Individual tumor growth kinetics of primary tumors receiving different pretreatments. (C) Photographs of the excised tumors. (D) Survival of mice in (B).

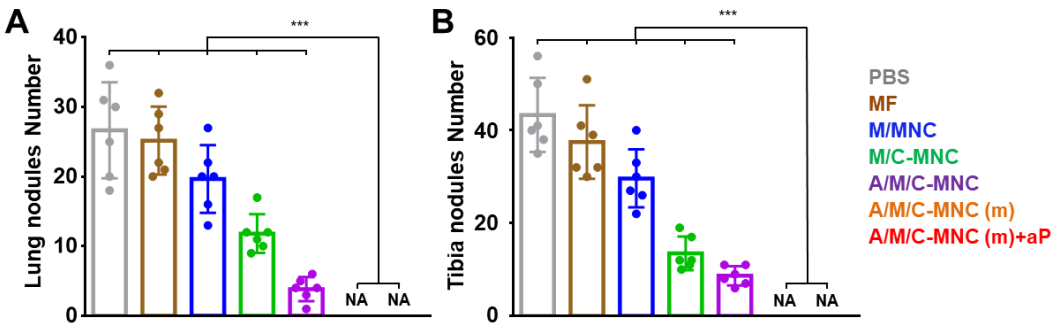

Figure S12. The number of tibia and lung metastatic foci in the therapeutic efficacy study after different treatments. (A) The number of lung metastatic foci. (**B**) The number of tibia metastatic foci. The average number of metastatic sites in both the tibias and lungs decreased in the order of PBS, MF, M/MNC, M/C-MNC, A/M/C-MNC, A/M/C-MNC(m) and A/M/C-MNC(m)+aP. Bars represent the mean ± s.d. (n=6).

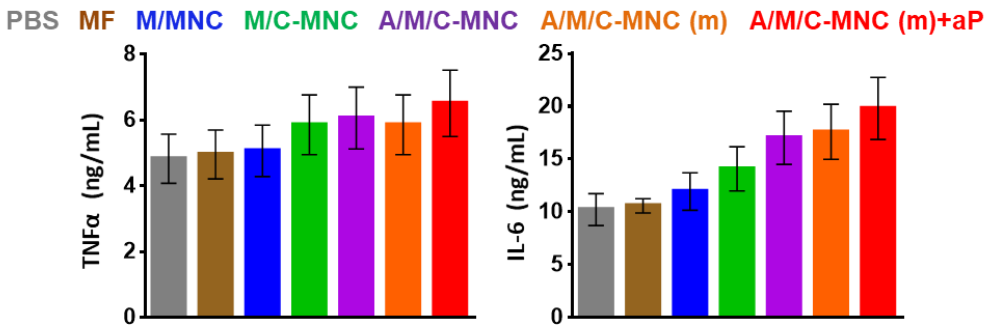

Figure S13. Amount of TNF-α and IL-6 released from mice receiving different treatments. The concentrations of both cytokines were within the normal range in all groups, indicating that the vaccine did not cause a cytokine storm. Bars represent the mean ± s.d. (n=6).

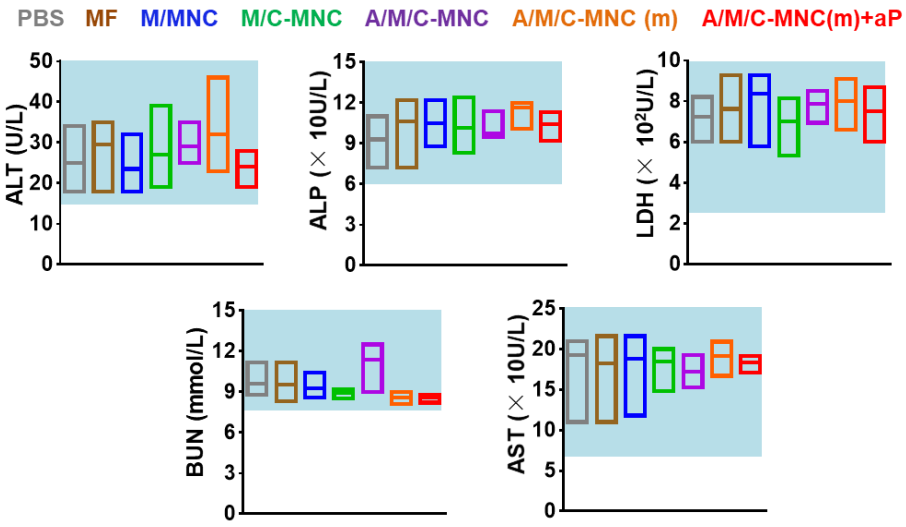

Figure S14. Side effect evaluation via serum biochemical parameter detection. All the markers including aspartate aminotransferase (AST), alanine aminotransferase (ALT), blood urea nitrogen (BUN), lactic dehydrogenase (LDH), and alkaline phosphatase (ALP) were within normal ranges, which further confirmed the safety of the vaccine. Bars represent the mean ± s.d. (n=6).

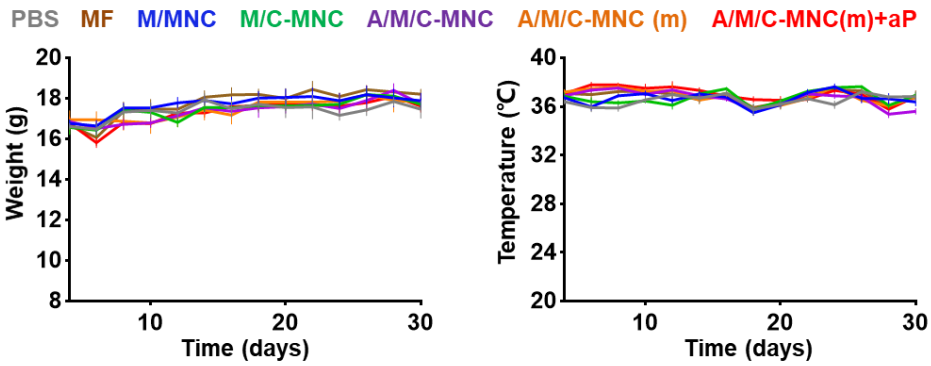

Figure S15. Weight and temperature change curves of mice receiving different treatments. There were almost no changes in all groups. Bars represent the mean ± s.d. (n=6).

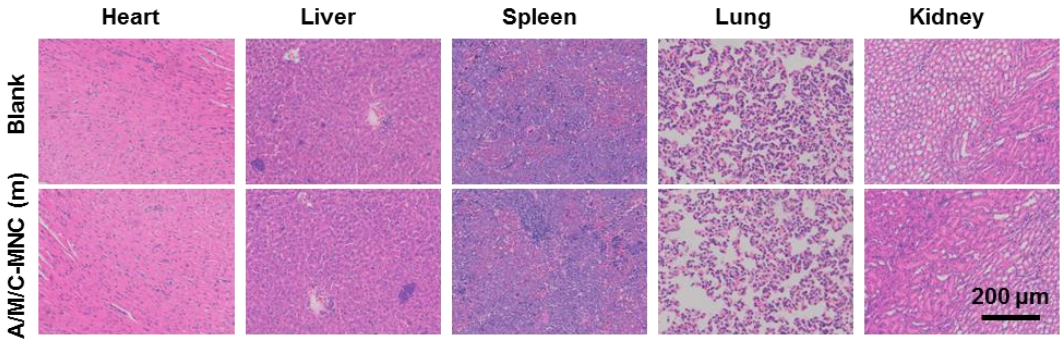

Figure S16. H&E stained tissue sections of the blank control and the A/M/C-MNC(m) groups. There were almost no differences between the two groups in all organs. Scale bar: 200 μm.